P7.3 INVESTIGATION OF CONDITIONAL SGS STRESS AND CONDITIONAL SGS STRESS PRODUCTION USING SURFACE LAYER (HATS) DATA

Qinglin Chen, Chenning Tong*
Department of Mechanical Engineering
Clemson University, Clemson, South Carolina 29634

1. INTRODUCTION

Large-eddy simulation (LES) computes the large scales, or resolvable scales of a turbulent flow and models the effects of the small, or subgrid-scales (SGS). When the filter scale is in the inertial range, the energy-containing scales are well resolved and most of the turbulent stresses is contained in the resolvable scales. The effects of small scales are generally considered to be limited to extracting the right amount of energy from the resolvable scales. Thus, the LES result is to some extent insensitive to the subgrid-scale model employed.

However, in large-eddy simulation of high Reynolds number turbulence boundary layers, such as the atmospheric boundary layer, the filter scale near wall region is inevitably in the energy-containing scales. This causes the near wall result to depend heavily on the SGS model. Therefore, an important question in improving SGS stress model is how the SGS stress effects the resolvable-scale velocity joint probability density function (JPDF) under these condition.

Previous studies of Pope (2000) and Langford and Moser (1999) have given the necessary and sufficient conditions for LES to correctly predict all multi-point JPDF of resolvable-scale velocity as that the conditional mean of the SGS stress conditional on the entire resolvable-scale velocity field must be reproduced by the modeled SGS stress.

In the present work, we study the influence of the SGS motion on the resolvable-scale statistics by analyzing the transport equation of the one-point joint probability density function (PDF) of the resolvable-scale velocity components, which can be derived following the method given by Pope (2000). The JPDF transport equation is given as

$$\begin{aligned}\frac{\partial f}{\partial t}+v_j\frac{\partial f}{\partial x_j} &= \frac{\partial^2}{\partial v_i\partial x_j}\{\langle\tau_{ij}|\mathbf{u^r}=\mathbf{v}\rangle f\}\\ &+ \frac{\partial^2}{\partial v_i\partial v_k}\{\langle-\frac{1}{2}P_{ij}|\mathbf{u^r}=\mathbf{v}\rangle f\}\\ &+ \frac{\partial^2}{\partial v_i\partial x_i}\{\langle p^r|\mathbf{u^r}=\mathbf{v}\rangle f\}\\ &+ \frac{\partial^2}{\partial v_i\partial v_k}\{\langle p^r\frac{\partial u_k^r}{\partial x_i}|\mathbf{u^r}=\mathbf{v}\rangle f\}\\ &+ \frac{g}{\Theta}\frac{\partial^2}{\partial v_3\partial v_i}\{\langle\theta^r u_i^r|\mathbf{u^r}=\mathbf{v}\rangle f\} \quad (1)\end{aligned}$$

where

$$\tau_{ij}=(u_iu_j)^r-u_i^ru_j^r$$

is the SGS stress. Transport due viscous force is generally small at high Reynolds numbers and is omitted from the equation. The SGS stress production rate P_{ij} is defined as

$$P_{ij}=-\{\tau_{ik}\frac{\partial u_j^r}{\partial x_k}+\tau_{jk}\frac{\partial u_i^r}{\partial x_k}\}$$

In the RHS of Eq. (1), we see that SGS stress effects velocity JPDF through transport by the SGS stress $\frac{\partial^2}{\partial v_i\partial x_j}\{\langle\tau_{ij}|\mathbf{u^r}=\mathbf{v}\rangle f\}$ both in physical and velocity space and in velocity the SGS stress production $\frac{\partial^2}{\partial v_i\partial v_k}\{\langle P_{ij}|\mathbf{u^r}=\mathbf{v}\rangle f\}$. Therefore, for LES to correctly predict the velocity JPDF, the conditional means of SGS stress, $\langle\tau_{ij}|\mathbf{u^r}\rangle$, and the conditional mean of the SGS stress production rate, $\langle P_{ij}|\mathbf{u^r}\rangle$, must be reproduced by the SGS model (Chen *et al.* (2003)).

The SGS stress production rate tensor P_{ij} can be decomposed as

$$P_{ij}=P_{ij}^d-\frac{2}{3}\tau_{kk}S_{ij} \quad (2)$$

where S_{ij} is the strain rate tensor of resolvable-scale velocity, P_{ij}^d is defined as

$$P_{ij}^d=-\{\tau_{ik}^d\frac{\partial u_j^r}{\partial x_k}+\tau_{jk}^d\frac{\partial u_i^r}{\partial x_k}\}$$

and $\tau_{ij}^d=\tau_{ij}-\frac{1}{3}\tau_{kk}\delta_{ij}$, is the deviatoric part of SGS stress. This decomposition can help us better understanding the physics of P_{ij}, because (1) P_{ij}^d is the production due to τ_{ij}^d, and $-\frac{2}{3}\tau_{kk}S_{ij}$ is the production due to τ_{kk}; (2) the normal components $P_{\alpha\alpha}$ ($\alpha=1,2,3$) of production rate contain the energy transfer from large-scale to small-scale, $P_{\alpha\alpha}^d$, and the inter-component redistribution among three normal components of the SGS stress, $-\frac{2}{3}\tau_{kk}S_{\alpha\alpha}$ ($-\frac{2}{3}\tau_{kk}S_{ii}$ is zero, indicating that the energy is redistributed among the three normal components of the SGS stress); (3) The shear components of P_{ij}^d ($i\neq j$) represents the production of shear stress due to straining and rotation acting on the anisotropic part of the SGS turbulence. The shear components $-\frac{2}{3}\tau_{kk}S_{ij}$ represents the production of shear stress due to straining of the isotropic part of the SGS turbulence.

In addition to the SGS stress production P_{ij}, the advection term $-u_k^r\frac{\partial\tau_{ij}}{\partial x_k}$ and the buoyancy production term P_{ij}^B also influence the evolution of SGS stress through the transport equation of the SGS stress, where $P_{ij}^B=\frac{g}{\Theta}\{\delta_{i3}[(\theta u_j)^r-\theta^r u_j^r]+\delta_{j3}[(\theta u_i)^r-\theta^r u_i^r]\}$. From the

*Corresponding author. E-mail: ctong@ces.clemson.edu

Table 1: Surface layer parameters of array 1 ($\Delta/z \approx 4$) for unstable cases

$\langle u \rangle (\mathrm{ms}^{-1})$	z/L	$u_* (\mathrm{ms}^{-1})$	$\epsilon (\mathrm{m}^2\mathrm{s}^{-3})$
3.13	-0.24	0.314	0.0311

definition of P_{ij}^B, we see that only three terms of buoyancy production rate are not zero. They are P_{13}^B, P_{23}^B and P_{33}^B, which correspond to SGS stress τ_{13}, τ_{23} and τ_{33} respectively. Thus, buoyancy production rate only effect τ_{i3} components.

2. HATS FIELD PROGRAM

The field measurements for this study were conducted as a collaboration among National Center for Atmospheric Research, Pennsylvania State University (C. Tong was part of the Penn State team), and Johns Hopkins University during the Horizontal Array Turbulence Study (HATS) field program. The HATS field measurement design was based on the transverse array technique proposed and studied by Tong *et al.* (1998) obtaining 2-D, horizontally filtered turbulence variables. The measurement setup consists of two arrays at two heights. The primary horizontal array has 9 equally-spaced sonic anemometers and the secondary parallel array has 5 sonic anemometers at a second height. The arrays are perpendicular to the prevailing wind direction. Both the resolvable-scale and SGS velocity and temperature can be measured using the arrays. The details of field program, which include the field site, instrumentation, data collection procedures, data quality, and accuracy etc., are documented in Horst *et al.* (2003).

3. RESULTS

In present study the unstable surface layer data are used. In order to reach a reasonable statistical convergency, we combined the results of qualified data sets collected by the same array configuration in different daytime. The averaged flow parameters are shown in table 1. The stability parameter z/L is approximate -0.24, where z is the height of the primary array and L is Monin-Obukhov length scale. Thus, we expect both buoyancy and shear to affect the results. Box filters are used to filter the data in both streamwise and crossstream direction. The filter size $\Delta/z \approx 4$, i.e., the filter size is in the energy containing scale. The other cases with different array configuration, i.e. different Δ/z and z/L are also computed. The results are qualitatively similar and are not shown here due to space limited.

The results for conditional SGS stress are normalized by the shear stress $u_*^2 = -\langle u'w' \rangle$. The result for conditional SGS stress production, buoyancy production and advection are normalized by the estimated dissipation rate $\epsilon = \phi_\epsilon \frac{u_*^3}{k_a z}$, where $k_a = 0.41$ and $\phi_\epsilon = 1 - z/L$ if $z/L \leq 0$ (as suggested by Kaimal *et al.* (1972)).

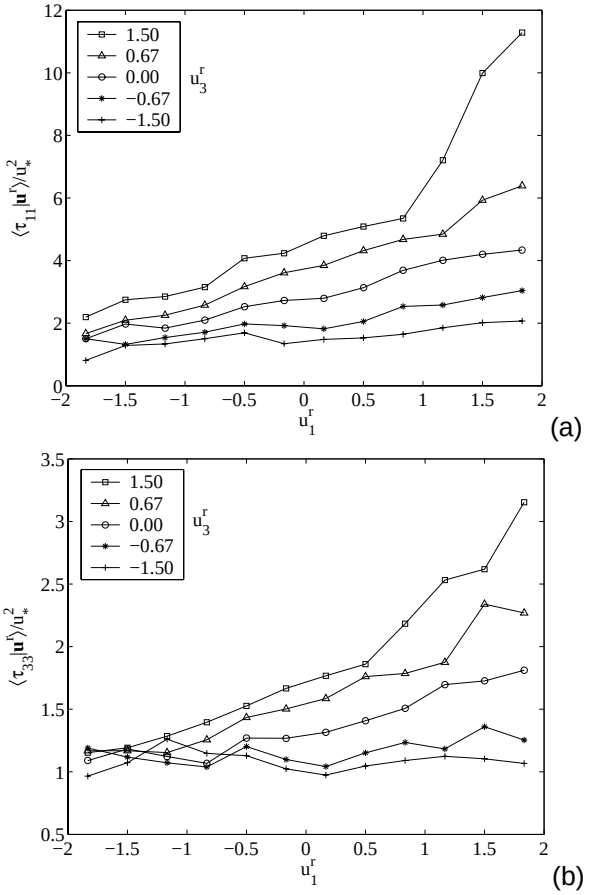

Figure 1: The conditional mean of SGS stress τ_{11} and τ_{33}

1. *Normal components of conditional SGS stress and its production rate*

The results for the conditional normal SGS stress components $\langle \tau_{11} | \mathbf{u^r} \rangle$ and $\langle \tau_{33} | \mathbf{u^r} \rangle$ are plotted against the horizontal resolvable-scale velocity, u_1^r, for different values of the vertical resolvable-scale velocity, u_3^r, and shown in figure 1 (a) and (b) respectively. Figure 1 shows that $\langle \tau_{11} | \mathbf{u^r} \rangle$ and $\langle \tau_{33} | \mathbf{u^r} \rangle$ generally increases with u_3^r. They also increase with u_1^r when u_3^r is positive, and depends weakly on u_1^r when u_3^r is negative, indicating that the dependence on u_1^r is enhanced by positive u_3^r. The dependence of $\langle \tau_{11} | \mathbf{u^r} \rangle$ can partly be attributed to vertical advection (Tong *et al.* (1999)). Figure 5 shows that the advection is generally positive for positive u_3^r and vice versa. In the surface layer the velocity variance varies slowly with the distance from the ground whereas the length scale is proportional to the distance; therefore the SGS eddies brought up from near the ground contain a large magnitude of SGS stress.

To better understand the trends for the conditional SGS normal stress, we postpone more detailed discussions of the normal SGS until after the results for the SGS stress production are presented. The results for the normal components of the conditional production rate $\langle P_{11} | \mathbf{u^r} \rangle$ and $\langle P_{33} | \mathbf{u^r} \rangle$, which are the energy transfer terms, are shown in figure 2 (a) and (b) respectively.

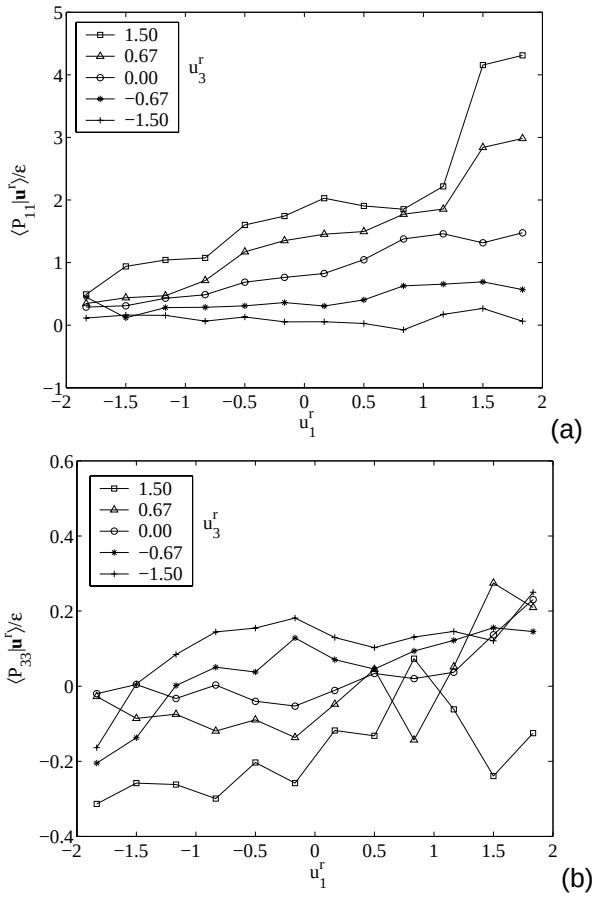

Figure 2: The conditional mean of SGS stress production rate P_{11} and P_{33}

Similar to $\langle\tau_{11}|\mathbf{u^r}\rangle$, $\langle P_{11}|\mathbf{u^r}\rangle$ also increases with u_3^r. It also increases with u_1^r and the dependence on u_1^r is enhanced by positive u_3^r and weakened by negative u_3^r. Figure 2 (b) shows that $\langle P_{33}|\mathbf{u^r}\rangle$ also increases with u_3^r and its dependence on u_1^r is generally weaker, especially for negative u_3^r.

To further understand the SGS production rate, we decompose $\langle P_{11}|\mathbf{u^r}\rangle$ and $\langle P_{33}|\mathbf{u^r}\rangle$ into $\langle P_{ij}^d|\mathbf{u^r}\rangle$ and $P_{ij}^k = -\frac{2}{3}\tau_{kk}S_{ij}$ (Eq. (2)). The results show that, when the resolvable-scale eddies move upward ($u_3^r > 0$) they are on average stretched in the vertical direction due to buoyancy acceleration, the conditional spectral transfer of $\langle P_{11}|\mathbf{u^r}\rangle$ and $\langle P_{33}|\mathbf{u^r}\rangle$ are positive, indicating forward energy transfer. The inter-component transfer terms have opposite signs, $\langle P_{11}^k|\mathbf{u^r}\rangle$ being positive and $\langle P_{33}^k|\mathbf{u^r}\rangle$ being negative, indicating τ_{33} loses energy to τ_{11}. When the resolvable-scale eddies associated with the returning flow of large convective eddies move downward ($u_3^r < 0$) they are on average compressed in the vertical direction due to the presence of the ground, the conditional spectral transfer, $\langle P_{11}^d|\mathbf{u^r}\rangle$, is still forward transfer but the conditional spectral transfer, $\langle P_{33}^d|\mathbf{u^r}\rangle$, is negative, indicating conditional backscatter, and the inter-component transfer terms have opposite signs, with $\langle P_{11}^k|\mathbf{u^r}\rangle$ being negative and $\langle P_{33}^k|\mathbf{u^r}\rangle$ being positive, indicating τ_{33} gains energy from τ_{11}.

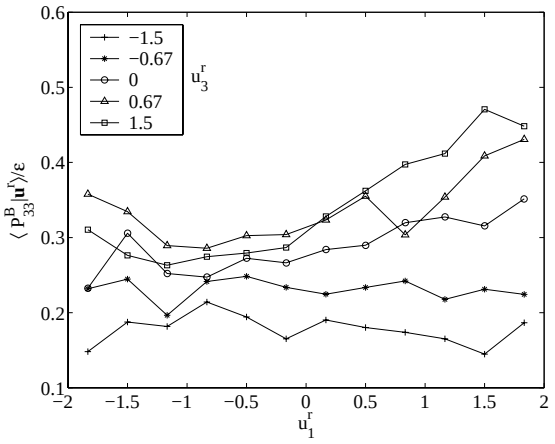

Figure 3: The conditional mean of buoyancy production rate of τ_{33}

The trends for $\langle P_{22}|\mathbf{u^r}\rangle$ (not shown) are generally similar to those of $\langle P_{11}|\mathbf{u^r}\rangle$. However, there are several differences. One difference is that $\langle P_{22}|\mathbf{u^r}\rangle$ increases with $|u_2^r|$, because the flow is symmetric in lateral direction. Another is that the magnitude of $\langle P_{22}|\mathbf{u^r}\rangle$ is smaller than that of $\langle P_{11}|\mathbf{u^r}\rangle$ and is negative when u_3^r has large negative values ($u_3^r < -0.6$) because the shear strain $\partial u_2^r/\partial x_3$ is smaller than $\partial u_1^r/\partial x_3$, resulting in smaller spectral transfer associated with shear compared to the case for $\langle P_{11}|\mathbf{u^r}\rangle$.

Because the evolution of $\langle\tau_{11}|\mathbf{u^r}\rangle$ is dominated by $\langle P_{11}|\mathbf{u^r}\rangle$, thus $\langle\tau_{11}|\mathbf{u^r}\rangle$ has similar trends to $\langle P_{11}|\mathbf{u^r}\rangle$. Similarly, the evolution of τ_{22} is dominated by P_{22}, thus $\langle\tau_{22}|\mathbf{u^r}\rangle$ (not shown) has similar trends to $\langle P_{22}|\mathbf{u^r}\rangle$. However, the trends of τ_{33} are different from those of P_{33}, because buoyancy production dominates the evolution of τ_{33}. Thus, $\langle\tau_{33}|\mathbf{u^r}\rangle$ has similar trends to the buoyancy production rate (shown in figure 3).

2. *Shear components of conditional SGS stress and its production rate*

The results for the conditional shear stress component $\langle\tau_{13}|\mathbf{u^r}\rangle$ is shown in figure 4 (a). The magnitude of $\langle\tau_{13}|\mathbf{u^r}\rangle$ generally increases with u_3^r. It also increases with u_1^r and the dependence is enhanced by positive u_3^r and weakened by negative u_3^r.

To further understand the result of $\langle\tau_{13}|\mathbf{u^r}\rangle$, we first discuss the result of $\langle P_{13}|\mathbf{u^r}\rangle$ (figure 4 (b)). Figure 4 (b) shows that the trends of $\langle P_{13}|\mathbf{u^r}\rangle$ are close to those of $\langle\tau_{13}|\mathbf{u^r}\rangle$, which generally increases with u_3^r. It also increases with u_1^r and the dependence is enhanced by positive u_3^r and weakened by negative u_3^r. The decomposition of $\langle P_{13}|\mathbf{u^r}\rangle$ into $\langle P_{13}^d|\mathbf{u^r}\rangle$ and $\langle P_{13}^k|\mathbf{u^r}\rangle$ (not shown) shows that the magnitudes of them both depend on u_1^r and the dependence is enhanced by positive u_3^r. The deviatoric production $\langle P_{13}^d|\mathbf{u^r}\rangle$ is positive indicating the negative production of the shear stress due to the straining and rotation in anisotropic turbulence. On the other hand, $\langle P_{13}^k|\mathbf{u^r}\rangle$ is negative and has about two times larger magnitude than $\langle P_{13}^d|\mathbf{u^r}\rangle$, indicating the positive production of shear stress due to the straining in isotropic turbulence.

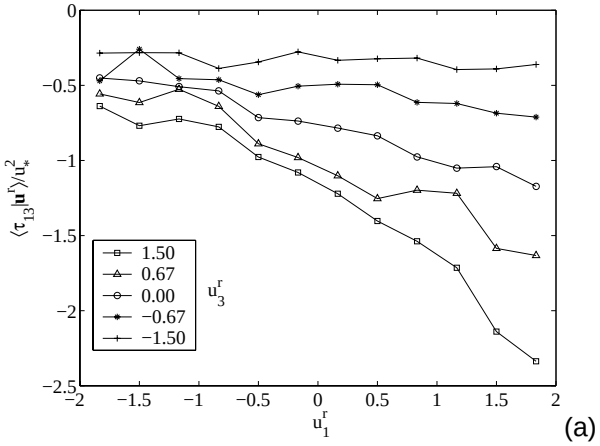

(a)

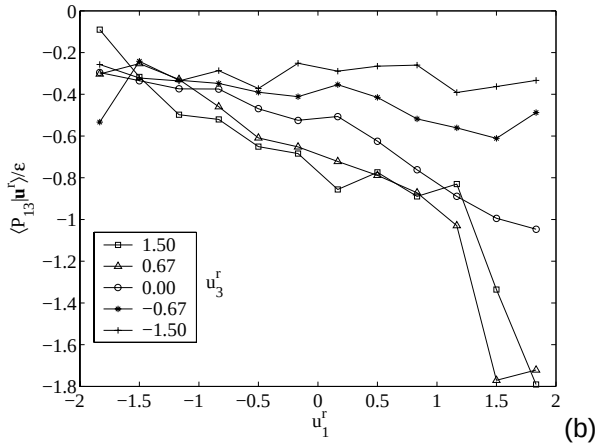

(b)

Figure 4: The conditional mean of the shear SGS stress component, τ_{13}, and its production rate

The trends of $\langle P_{23}|\mathbf{u^r}\rangle$ (not shown) are similar to those of $\langle P_{13}|\mathbf{u^r}\rangle$. The differences are that the magnitude of $\langle P_{23}|\mathbf{u^r}\rangle$ increases with $|u_2^r|$ because the flow is symmetric in the lateral direction, and that the magnitude of $\langle P_{23}|\mathbf{u^r}\rangle$ is smaller than that of $\langle P_{13}|\mathbf{u^r}\rangle$ because the shear of u_2^r is smaller than that of u_1^r in the vertical direction.

The evolution of $\langle \tau_{13}|\mathbf{u^r}\rangle$ is dominated by both $\langle P_{13}|\mathbf{u^r}\rangle$ and conditional buoyancy production $\langle P_{13}^B|\mathbf{u^r}\rangle$ (not shown), which has similar trends to $\langle P_{13}|\mathbf{u^r}\rangle$ but has only one half of the magnitudes of $\langle P_{13}|\mathbf{u^r}\rangle$. Therefore, $\langle \tau_{13}|\mathbf{u^r}\rangle$ has similar trends. Similarly, the evolution of $\langle \tau_{23}|\mathbf{u^r}\rangle$ (not shown) is dominated by both $\langle P_{23}|\mathbf{u^r}\rangle$ and buoyancy production $\langle P_{23}^B|\mathbf{u^r}\rangle$ (not shown) which has similar trends to $\langle P_{23}|\mathbf{u^r}\rangle$ but has only one half of the magnitudes of $\langle P_{23}|\mathbf{u^r}\rangle$. Therefore, $\langle \tau_{23}|\mathbf{u^r}\rangle$ has similar trends.

3. *Vertical advection*

Due to the limitation of the measurement technique employed, we can compute the advection only in the vertical direction. The advection of τ_{11} is shown in figure 5. From figure 5, we can see that the vertical advection of τ_{11} is positive with positive u_3^r and negative with negative u_3^r, but the magnitude of advection is relative small

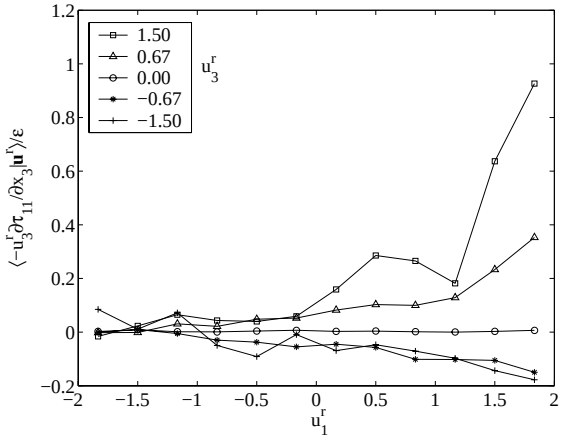

Figure 5: The conditional mean of the vertical advection of τ_{11}

to the production term. Thus, the advection effect the evolution of SGS stress but not as large as production.

4. *SGS stress model predictions*

As a first step to study the effects of SGS models on the JPDF of resolvable-scale velocity, we compute the predictions of the conditional stress and the conditional stress production rate using the Smagorinsky model (Smagorinsky (1963)) and the nonlinear model (Leonard (1974)). The Smagorinsky model is given by

$$\tau_{ij}^{smg} = -2(C_s\Delta)^2(\overline{S}_{ij}\overline{S}_{ij})^{1/2}\overline{S}_{ij}$$

where C_s is the model coefficient and is determined by matching the mean energy transfer rate, i.e., $C_s = \langle P_{ii}\rangle/\langle P_{ii}^{smg}\rangle$.

The conditional mean of the predicted results, $\langle \tau_{ij}^{smg}|\mathbf{u^r}\rangle$, is compared with the conditional mean of the deviatoric part of the SGS stress $\langle \tau_{ij}^{d}|\mathbf{u^r}\rangle$ obtained from data, because Smagorinsky model only models the deviatoric part of the SGS stress. The results of $\langle \tau_{ij}^{smg}|\mathbf{u^r}\rangle$ show that the Smagorinsky model cannot predicted either the conditional mean of SGS stress or its production rate well. For instance, even the best predicted SGS shear stress component $\langle \tau_{13}^{smg}|\mathbf{u^r}\rangle$ (figure 6 (a)) is severely unpredicted when compared with $\langle \tau_{13}|\mathbf{u^r}\rangle$ note that and $\tau_{13} = \tau_{13}^d$ (figure 4 (a)). The corresponding production rate $\langle P_{13}^{smg}|\mathbf{u^r}\rangle$ (figure 6 (b)) is even more poorly predicted, both in magnitude and trend by comparing with $\langle P_{13}^{d}|\mathbf{u^r}\rangle$ (figure 7).

Additional comparisons show that the standard Smagorinsky model generally predicts the trends of some shear stress components but not the normal components, and predicts the trends of some normal components of conditional SGS stress production rate but not the shear components. Further analyses (not discussed in detail here due to space limitation) show that although the evolution of $\langle \tau_{11}^{d}|\mathbf{u^r}\rangle$ involve $\partial u_1^r/\partial x_1, \partial u_1^r/\partial x_2$ and $\partial u_1^r/\partial x_3$, the shear strain rate component $\partial u_1^r/\partial x_3$ has the dominant contribution. However, $\langle \tau_{11}^{smg}|\mathbf{u^r}\rangle$ only contains $\partial u_1^r/\partial x_1$; therefore cannot correctly model the magnitude and the trend of $\langle \tau_{11}^{d}|\mathbf{u^r}\rangle$ ($\langle \tau_{22}^{smg}|\mathbf{u^r}\rangle$ is also

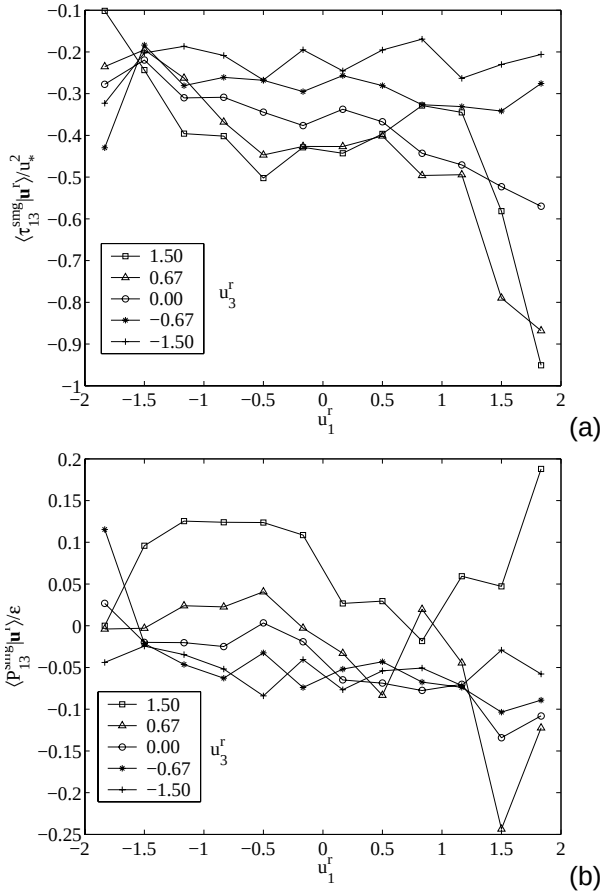

Figure 6: Modeled shear stress τ_{13}^{smg} and its production rate P_{13}^{smg} using the Smagorinsky model

similar). The vertical component $\langle \tau_{33}^{d} | \mathbf{u^r} \rangle$ is not correctly predicted by $\langle \tau_{33}^{smg} | \mathbf{u^r} \rangle$ because it dose not include the influence of buoyancy. The shear components $\langle \tau_{13} | \mathbf{u^r} \rangle$ and $\langle \tau_{23} | \mathbf{u^r} \rangle$ do not include the effects of buoyancy, therefore, their trends are better predicted.

The nonlinear model is given by

$$\tau_{ij}^{nl} = C_n \Delta^2 \frac{\partial u_i^r}{\partial x_k} \frac{\partial u_j^r}{\partial x_k}$$

where C_n is the model coefficient and is determined by matching the mean energy transfer rate, i.e., $C_n = \langle P_{ii} \rangle / \langle P_{ii}^{nl} \rangle$. The results show that the nonlinear model also cannot predicted both conditional SGS stress and its production rate at the same time. For example, figure 8 shows the conditional mean of modeled SGS stress $\langle \tau_{11}^{nl} | \mathbf{u^r} \rangle$ and the conditional mean of its production rate $\langle P_{11}^{nl} | \mathbf{u^r} \rangle$. Comparing $\langle P_{11}^{nl} | \mathbf{u^r} \rangle$ with $\langle P_{11} | \mathbf{u^r} \rangle$ (figure 2 (a)), we see that $\langle P_{11} | \mathbf{u^r} \rangle$ is generally correctly predicted, however, the $\langle \tau_{11} | \mathbf{u^r} \rangle$ (figure 1 (a)) is over predicted by approximately 50%.

More comparisons show that the normal SGS stress components are somewhat better predicted than the shear SGS stress components by the nonlinear model. On the other hand, the conditional mean of the SGS stress production rate are generally predicted. Therefore, the result show that the nonlinear model generally has better predictions than the Smagorinsky model. This can be understood in terms of the ingredients in the models. The result of $\langle \tau_{11}^{nl} | \mathbf{u^r} \rangle$ is better than $\langle \tau_{11}^{smg} | \mathbf{u^r} \rangle$ because it contains to $\partial u_1^r / \partial x_1, \partial u_1^r / \partial x_2$ and $\partial u_1^r / \partial x_3$ ($\langle \tau_{22}^{nl} | \mathbf{u^r} \rangle$ is also similar). However, $\langle \tau_{33}^{nl} | \mathbf{u^r} \rangle$ dose not include the dominated influence of buoyancy. Therefore, $\langle \tau_{33}^{nl} | \mathbf{u^r} \rangle$ is still not correctly predicted, although the prediction is better than that of the Smagorinsky model. Although $\langle \tau_{13}^{nl} | \mathbf{u^r} \rangle$ contains $\partial u_1^r / \partial x_3$, it also contains $\partial u_1^r / \partial x_1, \partial u_1^r / \partial x_3, \partial u_3^r / \partial x_3$ and but no buoyancy; therefore, the shear stress components predicted using the nonlinear model is not correct.

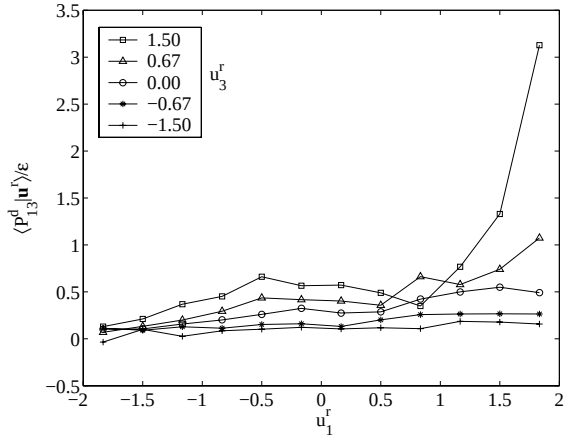

Figure 7: The conditional mean of deviatoric shear production rate P_{13}^{d}

The results for the Smagorinsky model and the nonlinear model suggest that SGS models based on only strain rate cannot predict both the conditional mean of SGS stress and its production well at the same time. Therefore, the SGS model need to be tested in the context of both conditional mean of SGS stress and the condtional mean of its production rate, because they both affect the JPDF of resolvable-scale velocity.

4. CONCLUSIONS

The subgrid-scale (SGS) stress in the atmospheric surface layer is studied using field measurements data. We analyze the conditional SGS stress and the conditional stress production rate conditional on the resolvable-scale velocity, which must be accurately modeled for large eddy simulation to reproduce the one-point resolvable-scale velocity statistics.

The results show that the normal conditional SGS stress generally increases with both the vertical and the streamwise velocity components. The magnitudes of the shear stress components also increase with the resolvable-scale vertical velocity. The conditional production is generally enhanced by positive vertical velocity and the conditional energy transfer is forward. Large negative vertical velocity, on the other hand, causes the energy transfer to decreases and could lead to conditional backscatter.

Buoyancy production and inter-component energy exchange are also shown to be important for the SGS

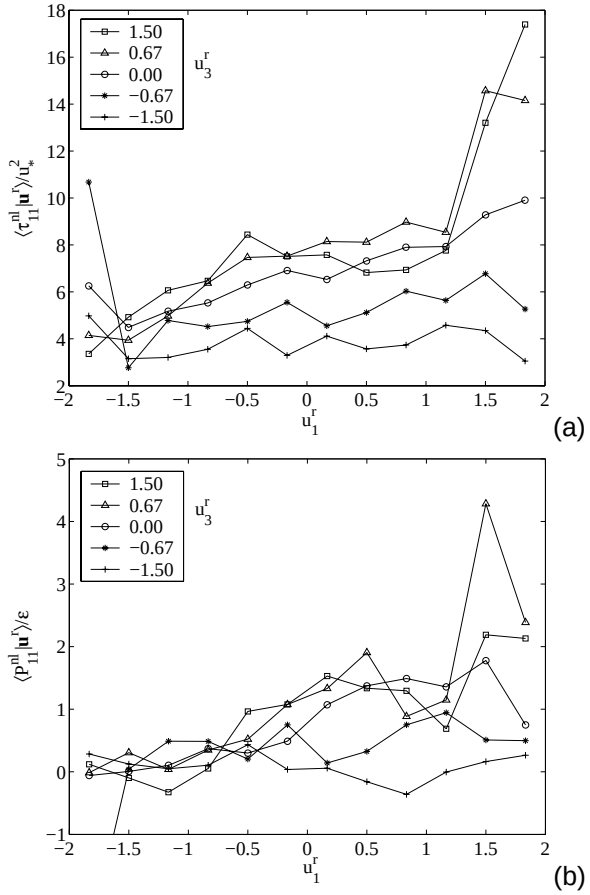

Figure 8: Modeled normal stress τ_{11}^{nl} and its production rate P_{11}^{nl} using the nonlinear model

stress evolution. Thus, the characteristic of conditional stress and conditional stress production rate are the result of interactions among buoyancy, SGS stress and the resolvable-scale strain.

Therefore, the characteristics of $\langle \tau_{ij} | \mathbf{u^r} \rangle$ and $\langle P_{ij} | \mathbf{u^r} \rangle$ are the result of interactions among buoyancy, SGS stress and resolvable-scale strain. The standard Smagorinsky and nonlinear model, which are based only on strain rate, can not correctly predict the $\langle \tau_{ij} | \mathbf{u^r} \rangle$ and $\langle P_{ij} | \mathbf{u^r} \rangle$. Therefore SGS model needs to be tested in the context of both $\langle \tau_{ij} | \mathbf{u^r} \rangle$ and $\langle P_{ij} | \mathbf{u^r} \rangle$. The results suggest that a model SGS stress transport equation has the potential to correctly predict both the conditional SGS stress and the conditional stress production rate.

References

Chen, Q., H. Zhang, D. Wang and C. Tong (2003). Subgrid-scale stress and its production rate: conditions for the resolvable-scale velocity probability density function. *J. of Turbulence* **4**, 027.

Horst, T. W., J. Kleissl, D. H. Lenschow, C. Meneveau, C. H. Moeng, M. B. Parlange, P. P. Sullivan and J. C. Weil (2003). HATS: Field observations to obtain spatially-filtered turbulence fields from transverse arrays of sonic anemometers in the atmosperic surface flux layer. *J. Atmos. Sci.* In press.

Kaimal, J. C., J. C. Wyngaard, Y Izumi and O. R. Coté (1972). Spectral characteristic of surface-layer turbulence. *Q.J.R. Met. Soc.* **98**, 563 – 589.

Langford, J. A. and R. D. Moser (1999). Optimal LES formulations for isotropic turbulence. *J. Fluid Mech.* **398**, 321 – 346.

Leonard, A. (1974). Energy cascade in large-eddy simulations of turbulent fluid flows.. *Adv. in Geophys.* **18**, 237 – 248.

Pope, S. B. (2000). Turbulent flows. *Cambridge University Press*.

Smagorinsky, J. (1963). General circulation experiments with the primitive equations. i: The basic experiment.. *Month Weather Rev.* **91**, 99 – 165.

Tong, C., J. C. Wyngaard and J. G. Brasseur (1999). Experimental study of the subgrid-scale stress in the atmospheric surface layer. *J. Atmos. Sci.* **56**, 2277 – 92.

Tong, C., J. C. Wyngaard, S. Khanna and J. G. Brasseur (1998). Resolvable- and subgrid-scale measurement in the atmospheric surface layer: Technique and issues. *J. Atmos. Sci.* **55**, 3114 – 26.